

Current Analysis

ADP current monitoring

Tidal and meteorologically-induced currents were measured during the study period. Only the months of December, January, and March provided useful data. Table 12 provides the summary data regarding the currents for those months. The currents contain a north-south diurnal oscillation as water moves in and out of Mobile Bay. The ADP was placed on the seabed in around 12.1 m (40 ft) of water some 914.4 m (3,000 ft) to the southwest of the mixed-sediment mound and 91.4 to 183 m (300 to 600 ft) to the southwest of the wave gage location (see Figure 24 and 54).

	Mean (m/s)	Maximum (m/s)	Std. Deviation (m/s)
December 1998	0.16	0.53	0.08
January 1999	0.19	0.82	0.10
March 1999	0.20	0.60	0.10

ADCP current monitoring

On 28 October 1999, current measurements were made using a boat mounted Acoustic Doppler Current Profiler (ADCP). A portion of the tidal cycle was measured with a 1,200-kHz and a 600-kHz Broadband ADCP manufactured by RD Instruments. These instruments measure current velocity by transmitting pulses of sound and measuring the Doppler shift of the reflected sound off matter suspended in the water. By time-gating the return signal and knowing the speed of sound in water, the ADCP associates different periods in the return signal with different ranges of depth known as bins. The water velocity for these depth bins was calculated by the TRANSECT software program provided by RD Instruments. A laptop computer was used on board the survey boat to interface the raw current data with the DGPS locations (Pratt and Stauble 2001).

The ADCP was mounted on the side of the survey boat with the instrument face always below the water surface. The bin resolution was set at 0.5 m (1.6 ft). Measurements were made remotely at regular intervals of time and space throughout the water column allowing generation of a cross-sectional current profile. The ADCP subtracts the vessel motion from the raw data to produce earth-referenced current vectors as the boat slowly traverses the survey line. HYPACK navigation software was used in conjunction with the DGPS to maintain survey line repeatability. Four different runs were made along a survey line running northeast to southwest across the mound area over a 9-hr portion of the tidal cycle. Other lines were also run over other portions of the SIBUA, so there was roughly a 2-hr space between runs over the mound. Portions of the ebb flow were measured in the morning and the beginnings of the flood flow were measured in the afternoon. The data were processed using the starting and ending points of the line for each run. The spatially referenced data were then imported

into HyPAS (Hydraulic Processes Analysis System) Pratt and Cook (2001) software inside ArcView. The data were depth-averaged to make the plots.

Figure 55 shows the current vectors for the four runs over the mixed-sediment mound. Run 1 at 09:18 CST on the ebb tide indicates the depth-averaged flow southwest out of the mouth of Mobile Bay. The average velocities ranged between 0.04 and 0.28 m/sec (0.40 and 0.93 ft/sec). Run 2 at 11:41 CST was closer to the end of the ebb flow and the depth-averaged velocity vectors turned more to the west. Flows ranged between 0.01 and 0.2 m/sec (0.32 and 0.70 ft/sec) at this point in the ebbing tide. Run 3 at 14:16 CST showed the flow changed more to the west from the Mobile Bay entrance at a time when the flow was changing from ebb to flood. Depth-averaged velocities slowed to between 0.03 and 1 m/sec (0.10 and 0.32 ft/sec). Run 4 at 17:51 CST during the beginning of the flood flow showed that the vectors turned to the northwest to flow back into the Mobile Bay entrance. Depth-averaged velocities dropped to a range from 0.07 to 0.15 m/sec (0.24 to 0.48 ft/sec) as the tide changed direction. Figure 56 shows the cross-section depth and horizontally distance-averaged velocity magnitude for the four runs over the ebb and transition to flood tidal flows. During the ebb flow (Runs 1 and 2), the highest velocities were measured near the surface ranging up to 0.64 m/sec (2.1 ft/sec), with lower flows (<0.24 m/sec (0.8 ft/sec)) below -4.57 m (-15 ft) mlw. As the tide switched from ebb to flood, the velocities slowed as the direction changed. Run 3 and 4 during the transition between ebb and flood, showed the highest velocities are still near the surface, between -1.52 and -3.01 m (-5 and -10 ft) mlw, but were reduced in magnitude. During all four runs, velocities increased slightly at the bottom near the mound and scour trough, but generally had the same direction as the depth-averaged flow, which was to the south to west depending on time in the tidal cycle. These bottom velocities are lower than the surface current, ranging between 0.18 to 0.52 m/sec (0.6 to 1.7 ft/sec), with the maximum measured during Run 2. The plots average every 61 m (200 ft) along the transect, so the values were averaged over several bin readings. The higher velocities near the bed could possibly be an artifact of the irregular bed and a few bad points in the bin just above the bed, but the raw data indicated that there are several bin readings of higher velocity near the bed around each averaged point.

From this limited data it appeared that the flood currents flow from the south and southwest into Mobile Bay over the mixed-sediment mound. On ebb, the flow is to the southwest out of the bay entrance. As the tide changes from ebb to flood and from flood to ebb, the flow rotates from the south to the north and back again in a westerly direction. From the data, the strongest flow is close to the surface and the bottom flows are low in the vicinity of the mound over most all of the tidal cycle. Little sediment transport at the mound is expected from tidal flows under normal conditions.

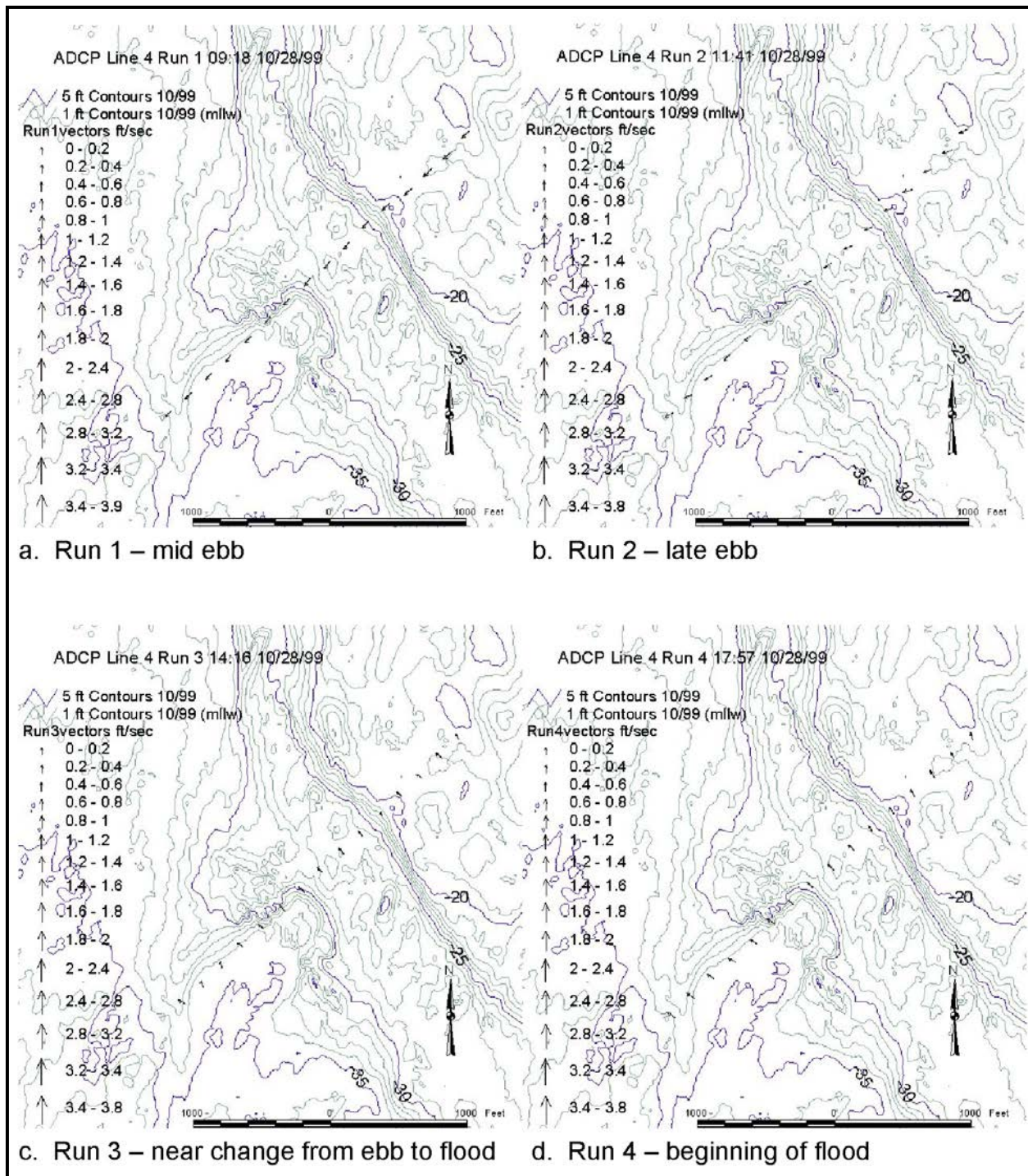


Figure 55. Map of depth-averaged ADCP current vectors along line 4 for 10/28/99 (To convert feet to meters, multiply by 0.3048)

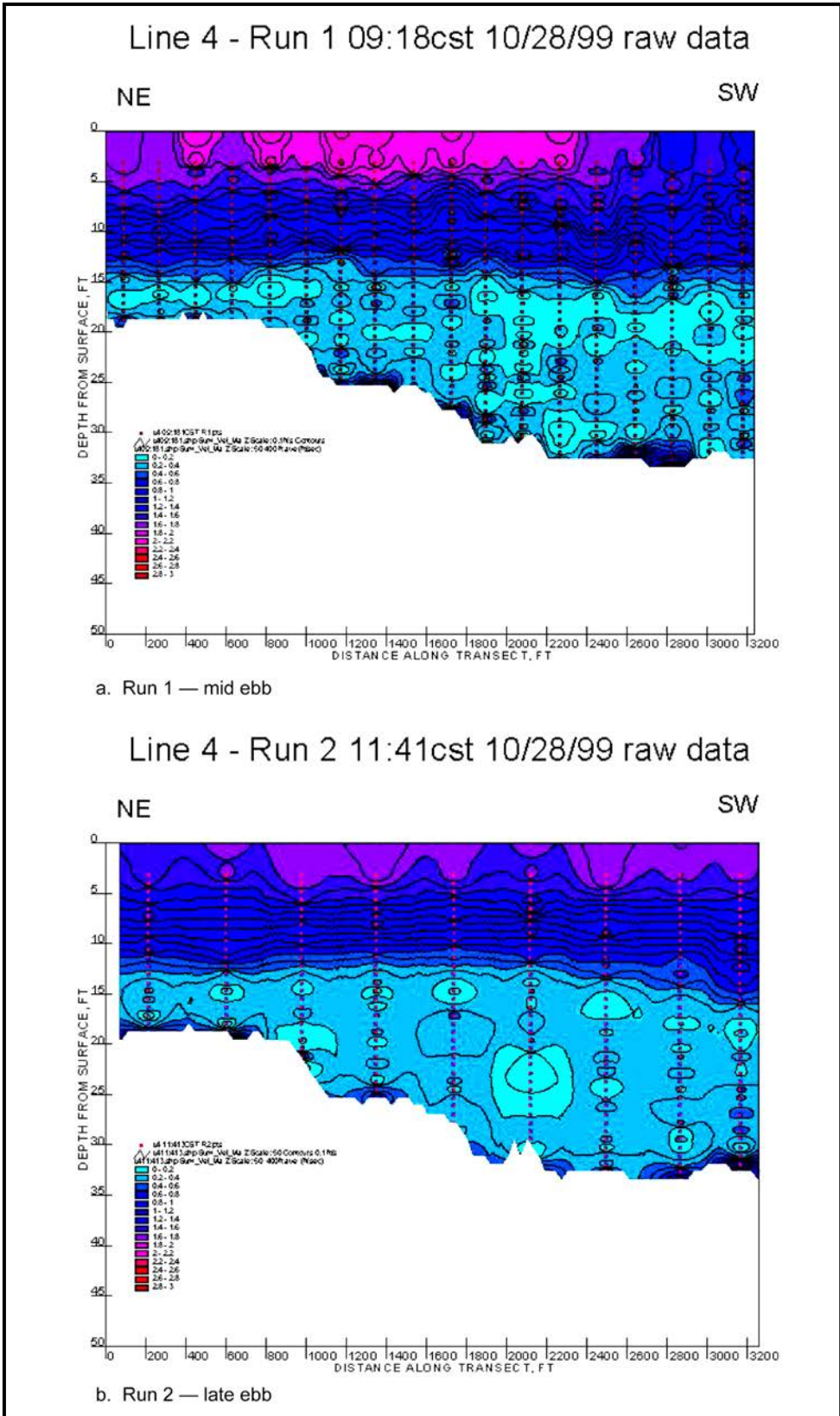
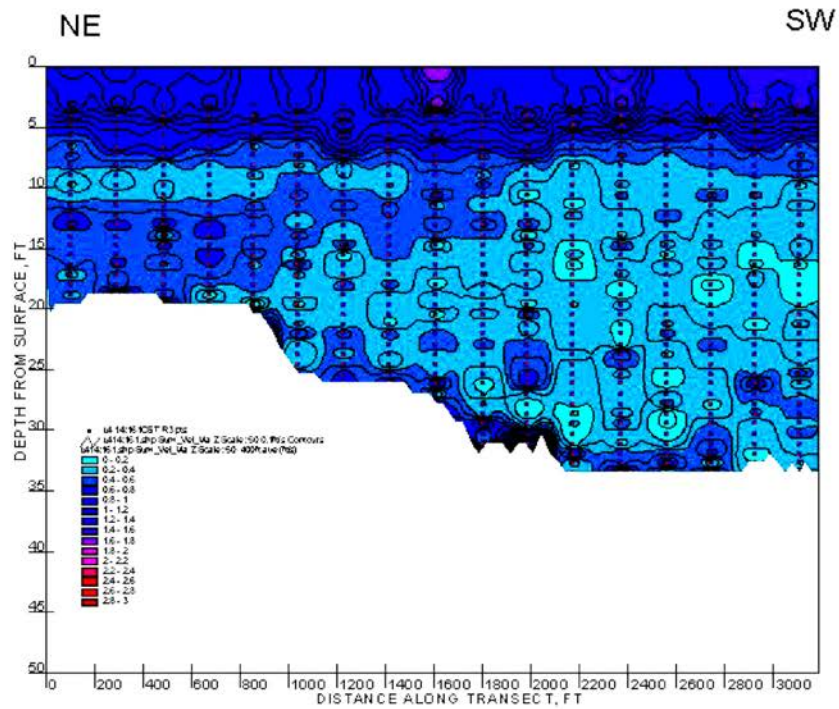


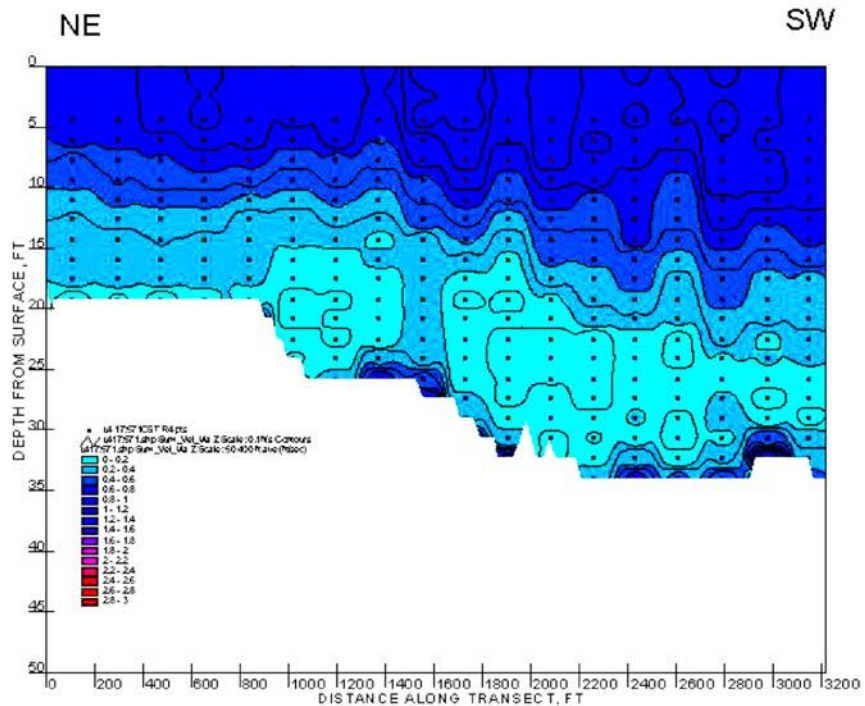
Figure 56. Cross-section plot of horizontally averaged ADCP current velocity along line 4 (To convert feet to meters, multiply by 0.3048) (Continued)

Line 4 - Run 3 14:16cst 10/28/99 raw data



c. Run 3 – near change from ebb to flood

Line 4 - Run 4 17:57cst 10/28/99 raw data



d. Run 4 – beginning of flood

Figure 56. (Concluded)

5 Erosion Rates and Bulk Properties of Dredged Sediments

Mixed sediments of sand, silt, and clay have significantly more complex erosion characteristics than pure sand or predominately sandy sediments. With the increase in fine grain material, there is a tendency of the particles to adhere to each other, and these mixed sediments are often referred to as cohesive. For sandy sediments, erosion is usually a function of grain-size distribution. However, erosion characteristics of mixed sediments cannot be described using the sandy sediment methods. Mixed sediment erosion rates can be affected not only by grain size, but also by bulk density, mineralogy, pore water chemistry, organic content, and presence of gas bubbles. One or more of these bulk properties may have an order of magnitude or more effect on erosion rates, depending on conditions. Insufficient data are presently available to quantify the effects of these parameters. When attempting to quantify erosion or dispersion characteristics of a mixed sediment bed, site-specific sediment erosion tests are required at significant cost and time. Because bulk density will affect erosion rates, these rates will change with depth below the sediment-water interface, adding an additional level of complexity to the site-specific experiments. This section will examine methods of associating sediment erosion rates to the dredged material's bulk properties.

A quantitative understanding of how sediment properties affect erosion rates would permit reasonable quantitative estimates of site dispersion without the presently required cost and time commitments of laboratory or field experiments. Therefore, under the DOER Program, the Corps has undertaken efforts to contribute to the existing database of sediment properties and erosion potentials. This will lead to a classification system for sediments that will assist in developing predictive models for the site of interest. From this database, the DOER Program will develop a method for classification of a site as highly, moderately, or minimally dispersive under known forcings (currents and waves) if the bulk properties of the sediments of interest are known. The effort to develop this database includes erosion and sediment property analyses of field samples and well-controlled laboratory samples.

The sediment dredged from the Mobile River includes a significant fraction of clay and silt particles and behaves in a cohesive manner. Visual inspection of the material indicated that it appeared to be high water content mud with some

sand evident. Information on the sediment bulk properties, erosion rates, and variation of erosion rates with depth below the sediment-water interface (bulk density) have been produced (Gailani et al. 2001).

Experimental Procedures

The measurements of erosion rates and bulk density were done at the University of California at Santa Barbara (UCSB) using Sedflume, a unique flume that can measure the erosion rates of sediments at high shear stresses comparable to those found in the nearshore during storms (up to stresses on the order of 20 N/m^2 (0.42 lb/ft^2)). Sedflume also has the capability to measure the variation in erosion rates with depth below the sediment-water interface (down to a meter or more). Although Sedflume is designed and has been used to measure the erosion rates of relatively undisturbed natural sediments from a field site, it can also be used to measure erosion rates of sediments that have been reconstructed in the laboratory to obtain sediments with well-defined properties. Further information on Sedflume can be found in McNeil, Taylor, and Lick (1996), Taylor and Lick (1996), and Jepsen, Roberts, and Lick (1997).

Sedflume (Figure 57) is essentially a straight flume that has a test section with an open bottom through which a rectangular cross-section coring tube containing sediment can be inserted. The main components of the flume are the coring tube, the test section, an inlet section for uniform, fully developed, turbulent flow, a flow exit section, a water storage tank, and a pump to force water through the system. The coring tube, test section, inlet section, and exit section are made of clear acrylic so that the sediment-water interactions can be

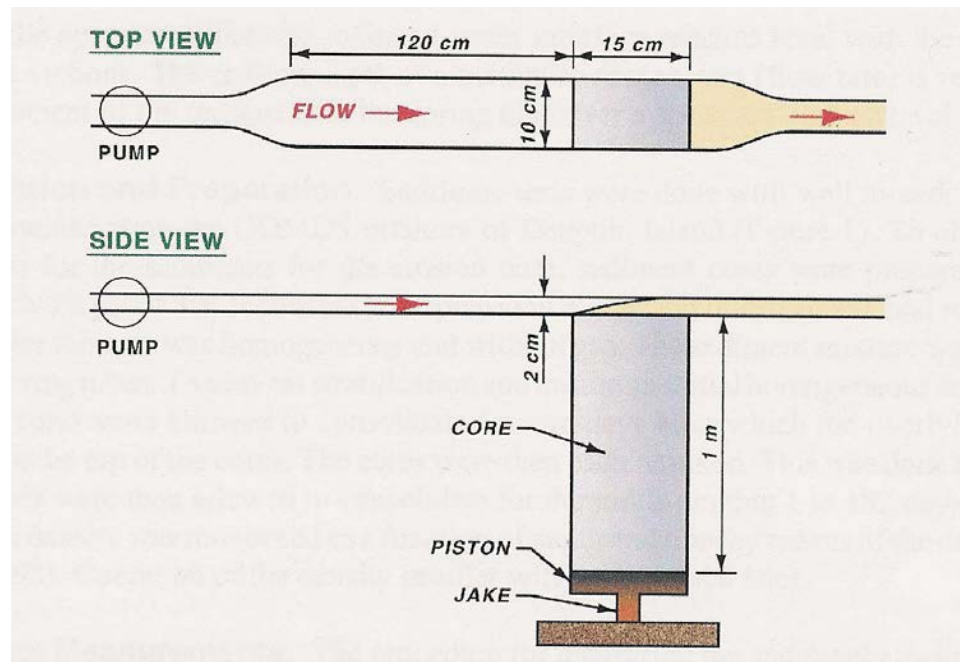


Figure 57. Schematic of Sedflume

observed. The coring tube has a rectangular cross-section, 10 cm by 15 cm (3.9 by 50 in.), and can be up to 1 m (3.28 ft) in length. Water is pumped through the system from a 500-L (0.32 gal) storage tank, through a 5-cm (2 in.) diameter pipe, and then through a flow converter into the rectangular duct shown. The flow converter changes the shape of the cross-section from circular to the rectangular duct shape while the cross-sectional area remains constant. The rectangular duct is 2 cm (0.79 in.) in height, 10 cm (3.94 in.) in width, and 120 cm in length; it connects to the test section, which has the same cross-sectional area and is 15 cm long. A three-way valve regulates the flow so that part of the flow goes into the duct while the remainder returns to the tank. There is a small valve in the duct immediately downstream from the test section that is opened at higher flow rates to keep the pressure in the duct and over the test section at atmospheric conditions.

Sedflume tests were done with well-mixed, reconstructed sediments obtained from the mixed-sediment mound at the five locations during the immediate post-placement field sediment collection in December 1998. Several 37.85 L (10-gal) buckets were filled with sediment collected by the bucket dredge at each site. These buckets were transported to the laboratory. At the start of each test, the coring tube was filled with reconstructed sediments, which were prepared using approximately 75.7 L (20 gal) of wet sediments that were placed in a 113.6-L (30-gal) cylindrical tank and mixed until the sediment-water mixture was homogeneous and without gas. The sediment mixture was then poured into 20-cm coring tubes. To prevent stratification and ensure an initial homogeneous sediment/water mixture, the cores were allowed to consolidate for two days after which the overlying water was removed from the top of the cores. The cores were then each remixed. This was done twice for each core. The cores were then allowed to consolidate for durations ranging 1 to 182 days. During this time, the bulk density was monitored as a function of depth and time by means of the density profiler.

The coring tube and the sediment it contains are inserted into the bottom of the Sedflume test section. An operator moves the sediment upward using a piston inside the coring tube and connected to a hydraulic jack with a 1-m (3.28-ft) drive. The jack is driven by the release of pressure regulated with a switch and valve system. By this means, the sediments can be raised and made level with the bottom of the test section. The movement of the jack can be controlled in measurable increments as small as 0.5 mm (0.01 in.). Water is forced through the duct and the test section over the surface of the sediments. The shear stress produced by this flow causes the sediments to erode. As the sediments in the core erode, they are continually moved upwards by the operator so that the sediment-water interface remains level with the bottom of the test and inlet sections. The erosion rate is recorded as the upward movement of the sediments in the coring tube over time.

Measurements of Erosion Rates

A measurement was made of the depth to the bottom of the sediment in the core. The flume was then run at a specific flow rate corresponding to a particular

shear stress. Erosion rates were obtained by measuring the remaining core length at different time intervals, taking the difference between each successive measurement, and dividing by the time interval.

The following procedure was used to measure erosion rates at multiple shear stresses using data for an individual core. Starting at a low shear stress, the flume was run sequentially at higher shear stresses with each succeeding shear stress being twice the previous one. Generally, about three to five shear stresses were run sequentially. Each shear stress was run until at least 0.5 to 1.0 mm (0.01 to 0.04 in.), but no more than 2 cm (0.79 in.), was eroded. The time interval was recorded for each run with a stopwatch. The flow was then increased to the next shear stress, and so on until the highest shear stress was run. This cycle was repeated until all of the sediment had eroded from the core. If after three cycles a particular shear stress showed a rate of erosion less than 2×10^{-5} cm/s (6.6×10.7^{-7} ft/sec), it was dropped from the cycle; if after many cycles the erosion rates decreased significantly, a higher shear stress was included in the cycle.

Measurements of Critical Shear Stress for Erosion

From previous experiments in the Sedflume (Jepsen, Roberts, and Lick 1997), it was determined that, for each type of sediment, the erosion rate was a unique function of the bulk density and shear stress and could be approximated by

$$E = A \tau^n \rho^m \quad (1)$$

where E is the erosion rate (cm/s); τ is the shear stress (N/m^2); ρ is the bulk density (g/cm^3); and A , n , and m are constants that depend on the type of sediment and include the effects of the bulk properties (other than bulk density) previously listed.

A critical shear stress can be quantitatively defined as the shear stress at which a very small, but accurately measurable, rate of erosion occurs. In the present study, this rate of erosion was chosen to be 1×10^{-4} cm/s, 3.3×10^{-6} ft/s) representing approximately 1 mm (0.04 in.) of erosion in 15 min. Since it would be difficult to measure all critical shear stresses at exactly 1×10^{-4} cm/s, erosion rates were generally measured above and below 1×10^{-4} cm/s (3.3×10^{-6} ft/s) at shear stresses, which differ by a factor of two. The critical shear stress was then linearly interpolated to an erosion rate of 1×10^{-4} cm/s (3.3×10^{-6} ft/s). This method provides results with approximately 20 percent accuracy for the critical shear stress. Alternatively, the value of τ_c can be determined directly from Equation 1, which, after rearranging becomes

$$\tau_c = \left(\frac{E}{A} \right)^{1/n} \rho^{-m/n} \quad (2)$$

where $E = 1 \times 10^{-4}$ cm/s and the constants A , n , and m are determined from the erosion experiments.

Bulk Properties Measurements

To assess the parameters that affect sediment erosion, bulk properties including bulk density, water content, median particle size, organic content, and sediment gas volume were determined as a function of depth. Sediment bulk densities were measured nondestructively as a function of depth by means of the density profiler (Gotthard 1998). The density profiler gives a detailed, non-destructive measurement of bulk density. Only a few grams of sediment are needed for measuring the other bulk parameters, so small amounts of sediment were removed during the erosion tests at various depths within the core for these measurements. This procedure eliminates the use of duplicate cores, one for bulk properties and one for erosion tests.

The density profiler uses a gamma radiation emitter, ^{137}Cs , as a radiation source and measures the attenuation of the radiation as it is transmitted horizontally through the sediments. Once the transmitted radiation is measured, this can be directly related to density of the sediments in the core (Gotthard 1998). The density profiler measures the actual sediment density, including solids, water, and any gas present. In contrast, the standard procedure for measuring sediment density measures the sediment density due to solids and water, and ignores the presence of gas. In this study, by measuring both densities, the gas volume in the sediments can be determined.

The standard procedure for determining density as used here begins with slicing the sediment cores into 1- to 2-cm sections and weighing them to get a wet weight (m_w). They are then dried in the oven at approximately 75 °C (167 °F) for 2 days and weighed again to get a dry weight (m_d). In terms of m_w and m_d , the moisture content, W , is given by

$$W = \frac{m_w - m_d}{m_w} \quad (3)$$

This procedure generally eliminates any gas originally present in the sediments. The bulk density as determined by this method, $\rho^*(\text{g}/\text{cm}^3)$, is related to the moisture content by

$$\rho^* = \frac{\rho_s \rho_w}{\rho_w + (\rho_s - \rho_w)W} \quad (4)$$

where $\rho_s = 2.6 \text{ g}/\text{cm}^3$ and is the density of the solid particles, and $\rho_w = 1.0 \text{ g}/\text{cm}^3$ and is the density of the water.

From their definitions, $\rho^* = m_{sw}/V_{sw}$ and $\rho = m_{sw}/(V_{sw} + V_g)$, where m_{sw} is the mass of the solids and water, V_{sw} is the volume of the solids and water, and V_g is the volume of the gas within the sediments. The total volume, V , is given by $V_{sw} + V_g$. From these definitions, the fractional gas volume, $v_g = V_g/V$, can be shown to be

$$v_g = \frac{\rho^* - \rho}{\rho^*} \quad (5)$$

Particle sizes and particle-size distributions were determined by use of a Malvern particle sizer for particle diameters between 0.5 and 600 μm (11 and 0.74 phi). All sediment samples had particle sizes less than 600 μm (0.74 phi). A small amount of sediment was mixed with water and disaggregated in a Waring blender. Approximately 1 ml (0.002 pts) of this solution was then used for analysis by the particle sizer. From these measurements, the median and the distribution of grain sizes as a function of depth were obtained.

The organic carbon content was determined by extracting approximately 5 ml (0.01 pts) of the sediment water mixture that was disaggregated in the Waring blender as previously described above and then drying it in an oven at 75 °C (167 °F). The dry sediment was crushed into powder and weighed. Approximately 5 ml (0.01 pts) of 10 percent hydrochloric acid was added to every 1 g (0.04 oz) of dry sediment. The sample was again dried in the oven at 75 °C (167 °F) and analyzed in a Leeman Labs Model 440 CHN Analyzer at the UCSB Marine Science Analytic Laboratory to determine the total organic carbon content of the sediment.

The mineralogy of the sediments was approximately determined by means of X-ray powder diffraction by Reed Glasmann (Willamette Geological Service, Philomath, OR). The measurements for the field sediments were taken at depths of 5 to 10 cm (27 to 39 in.). The clay-size (< 2 μm (9 phi)) and finer silt-size (2 to 15 μm (9 to 6 phi)) fractions of the sediments had high concentrations of clay minerals. In the clay-size fraction, the minerals were primarily smectite (the most cohesive of the clays), illite, and kaolinite. Of the total sediment mass, it is estimated that the smectite mass was about 8 percent.

Measurements were also made of the water soluble and exchangeable fractions of manganese (Mn^{2+}) and iron (Fe^{2+} and Fe^{3+}) by means of extraction with ammonium acetate. This was done by the Marine Science Analytical Laboratory at UCSB. Mn^{2+} concentrations were determined to be approximately 84 $\mu\text{g Mn}^{2+}/\text{g}$ dry sediment. Exchangeable manganese concentrations were much greater than exchangeable iron concentrations for the Mobile River sediments placed on the mound.

General Sediment Characteristics

Bulk properties and erosion rates were measured for well-mixed (or reconstructed) sediments from all five sites. A summary of this data is shown in

Table 13 which lists the median particle size (D_{50}), organic content, gas fraction (for long time), bulk density after 60 days of consolidation, the critical shear stress for erosion, and the coefficients A , n , and m for Equation 1 for all sites. The averages of these quantities over all five sites are also listed.

Site	D_{50} μm	Organic Content %	Gas Fraction %	Density at 60 d g/cm^3	τ_c N/m^2	A	n	m
PD1	21.0	1.12	1.20	1.48	1.27	3.5×10^{17}	3.46	-132
PD2	19.6	1.37	0.73	1.48	1.20	----	----	----
PD3	21.7	1.09	1.10	1.49	1.84	2.0×10^{31}	2.00	-207
PD4	20.8	0.55	1.05	1.49	1.60	1.8×10^{31}	3.06	-209
PD5	22.4	0.87	1.05	1.52	1.74	4.3×10^{16}	4.16	-126
Average	21.1	1.0	1.03	1.49	1.53	----	----	----

The median particle sizes were about 21 μm (5.57 phi) with little deviation between sites. Organic contents were low (1.0 percent) compared to other sites investigated. Because of the low organic contents, gas fractions were also low (1.0 percent). Densities for all sediments were similar; they increased with time, but at 60 days, they were about 1.49 g/cm^3 (93.01 lb/ft^3). The critical shear stresses for erosion were very high, approximately 1.5 N/m^2 (0.03 lb/ft^2), and significantly higher than τ_c for other sediments that we investigated, which generally varied from 0.1 to 0.4 N/m^2 (0.002 to 0.008 lb/ft^2). The major reason for these high values is the oxidation reaction at the sediment-water interface and will be discussed further in the following section.

General Erosion Characteristics

After thorough mixing, the sediments throughout the cores were uniform in color, texture, general appearance, and particle size. However, in times of a few minutes to a few hours after deposition, a thin layer of lighter-colored sediment began to form at the sediment-water interface. As time increased, the thickness of this layer increased to about 5 to 7 mm (0.2 to 0.28 in.) after 60 days of consolidation. The density of this layer was significantly lower (about 1.35 g/cm^3 (84.24 lb/ft^3)) than that of the darker sediment below (about 1.5 g/cm^3 (93.63 lb/ft^3)); the density of these darker sediments increased slightly with depth. This light-colored surficial layer was due to the relatively high concentration of the manganese ion, Mn^{2+} , in the reduced zone of the sediment and the precipitation of this ion in the form of manganese dioxide as the surface was exposed to oxygen that was present in the overlying water. This precipitate acted to cement the surficial layer.

The surficial layer, after oxidation, was very difficult to erode. The average critical shear stress for erosion was about 1.5 N/m^2 (0.03 lb/ft^2) and was much greater by about a factor of two than τ_c for the sediments below this layer and

also much greater than τ_c for other sediments that we have observed and measured. At or somewhat above the critical shear stress, the surficial, oxidized sediments typically would experience no erosion for a few minutes and would then fail catastrophically with up to 2 cm (0.79 in.) of sediment eroding almost instantaneously. This rate could not be quantified and only τ_c was recorded. The erosion rates for sediments below this layer were quantified.

Sediments at depth would occasionally also erode in a catastrophic mode. In some cases, the reason was evident and was due to the oxidation of the surficial sediments; this required low erosion rates so that the diffusion of the oxidation reaction into the sediments was faster than the removal of sediments by erosion. In this case, an oxidized layer could form and catastrophic erosion then resulted. Below this oxidized layer, the erosion process was generally similar to that in other cohesive sediments investigated. For small compaction times and low shear stresses, erosion primarily occurred as particles, aggregates, or small chunks of sediment less than 1 mm (0.004 in.) in diameter. As consolidation time and shear stresses increased, the sediments began eroding more as large chunks, ranging from about 1 mm up to 5 mm (0.004 to 0.020 in.) with some chunks even larger. Occasional catastrophic erosion (on the order of 1 cm (0.34 in.) of sediments) occurred for large times when the sediments were quite cohesive and the shear stresses were large.

Bulk Properties and Erosion Rates

Bulk parameters and erosion rates for all five sites were similar. Therefore, only sediments from one site, PD1, will be discussed in detail. Results for the bulk density as a function of depth are shown in Figure 58. Although more profiles were taken, for purposes of clarity, only the profiles for 3 hr and 2, 8, 32, 64, 90, and 167 days are shown. In all of the experiments, the density was relatively low at the surface in a thin layer a few centimeters thick and then increased with depth. As time increased, the density at the surface increased and also increased more rapidly with depth. This is due to water migrating upwards and out of the sediments because of the weight of the overlying sediment. Effects of gas on the density are minimal.

The densities shown in the previous figure were obtained from 1-cm (0.34-in.) averages of data from the density profiler. For comparison, the densities as a function of depth at 64 days averaged over 0.1 and 1.0 cm (0.03 and 0.34 in.) are shown in Figure 59. The density averaged over only 0.1 cm (0.03 in.) shows relatively large variations; this is primarily due to variations in the density of the solid-water matrix, ρ^* , since the gas fraction is less than 1 percent. The density, ρ^* (averaged over 1 cm (0.34 in.)), is also shown as a function of depth.

From ρ and ρ^* , the gas fraction was determined and is shown as a function of depth at different time intervals in Figure 60. There are significant variations in the gas fraction at any particular time, but it can be seen to increase with time, with a reasonably steady-state average at longer time periods (i.e., 60 days) of

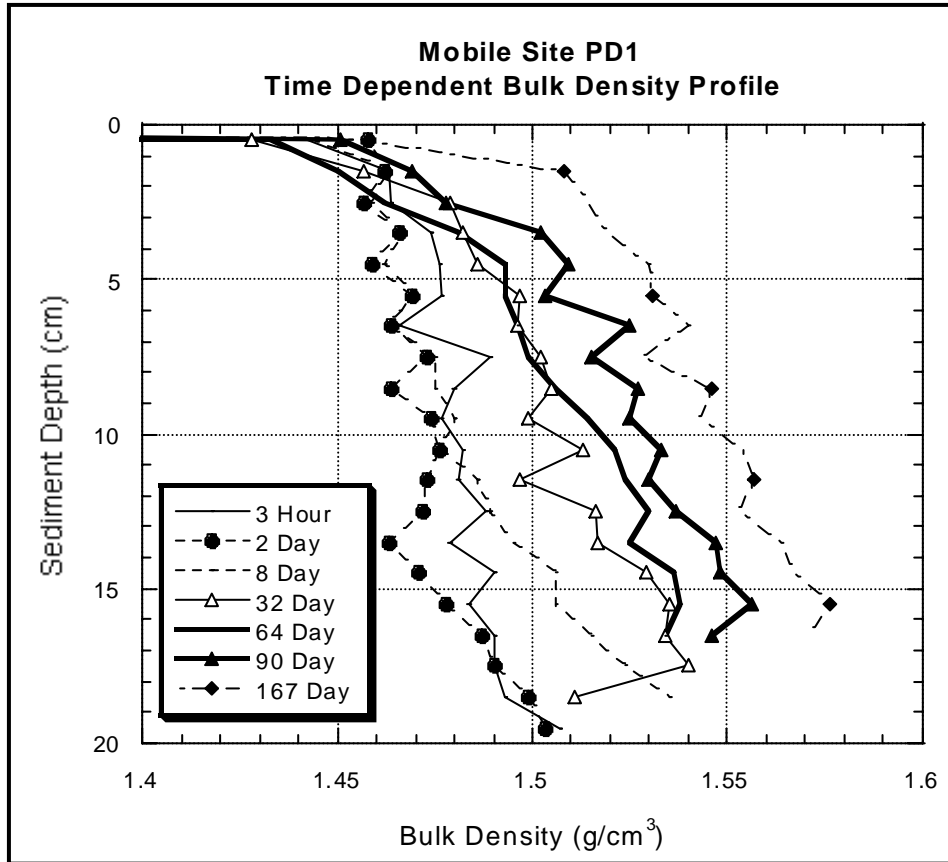


Figure 58. Bulk density as a function of depth at times after deposition of 3 hr and 2, 8, 32, 64, 90, and 167 days

between 1 and 2 percent. This is relatively small by comparison with gas fractions in other sediments investigated.

Erosion rates as a function of depth with shear stress as a parameter are shown in Figure 61 for times of 1, 30, 60, and 182 days of consolidation. Erosion rates shown are for the sediments below the oxidized layer. For these sediments, it can be seen that erosion rates increase rapidly with shear stress. Erosion rates also tend to decrease with depth due to the consolidation of sediments with depth. For a particular shear stress, erosion rates decrease with time by almost three orders of magnitude over the period of 182 days. The rate of decrease in erosion is large initially (i.e., between 1 and 30 days). The rate of decrease in erosion is less for the longer time periods because the sediment is almost fully consolidated (i.e., between 60 and 182 days).

Erosion rates as a function of density with shear stress as a parameter are shown in Figure 62. The data is well represented by Equation 1, i.e., (a) for each shear stress, a straight line can approximate the data, and (b) the straight lines are equidistant. For this case, $A = 1.2 \times 10^{14}$, $n = 3.46$, and $m = 132$. These rates are significantly lower than those in sediments we have investigated previously, by as much as an order of magnitude. The major cause of this reduction is the presence of smectite at a concentration of 8 percent. Although the effects of

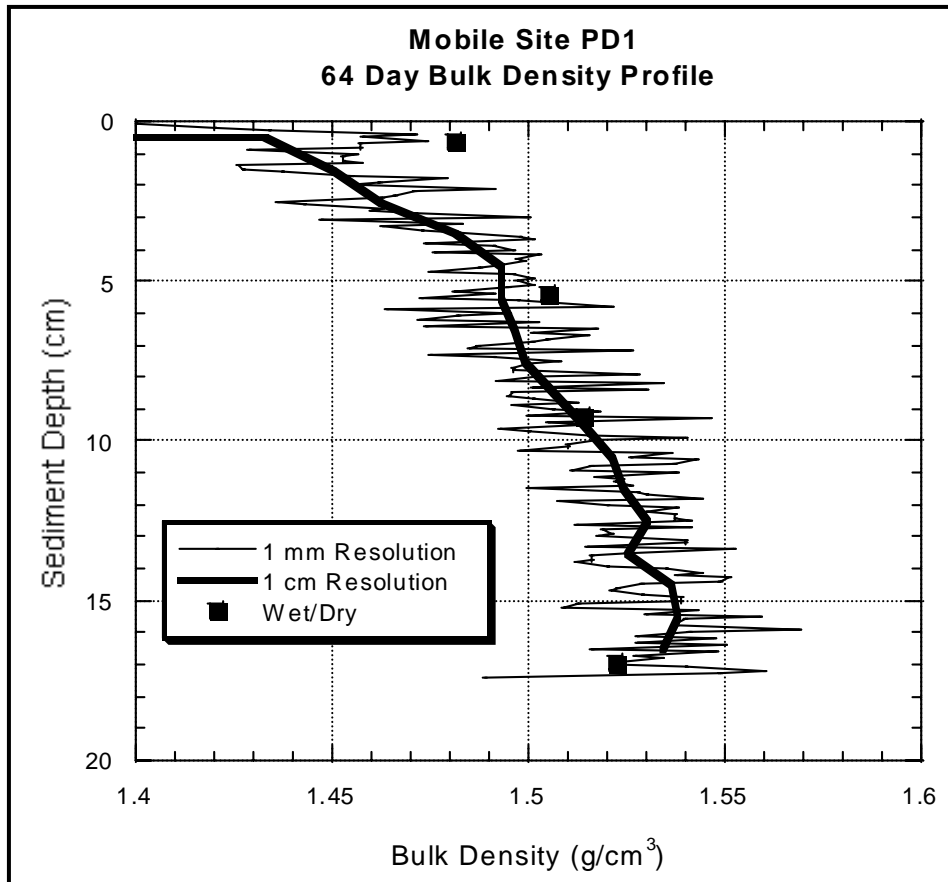


Figure 59. At 64 days, density of the solid-water matrix, ρ^* (averaged over 1 cm), as well as bulk density, ρ , at 0.1- and 1.0-cm averages as a function of depth

smectite have not been investigated directly, the effects of smectite should be quantitatively similar to those of bentonite. This amount of bentonite has been shown by Jin, McNeil, and Lick (2000) to be sufficient to decrease erosion rates by about two orders of magnitude compared with erosion rates of the same sediment without bentonite.

Effects of bentonite on erosion rates have been previously examined by Jin, McNeil, and Lick (2000); however, the effects of other clay minerals have not been quantitatively determined, but need to be in order to more quantitatively understand the effects of clay minerals. No systematic and/or quantitative investigations of the effects of manganese and iron oxidation and precipitation on erosion rates have been made; however, because of the large increase in the critical shear stress caused by this process, this needs further investigation.

The implications of the effects of smectite on erosion rates are significant when developing predictive models for site dispersion. If relationships are quantitatively known, then simple mineralogy tests of sediment scheduled for dredging could indicate if that material is minimally erosive. Ongoing research (Jin, McNeil, and Lick 2000) has indicated that the presence of bentonite (a member of the smectite family) will significantly reduce erosion rates. If further

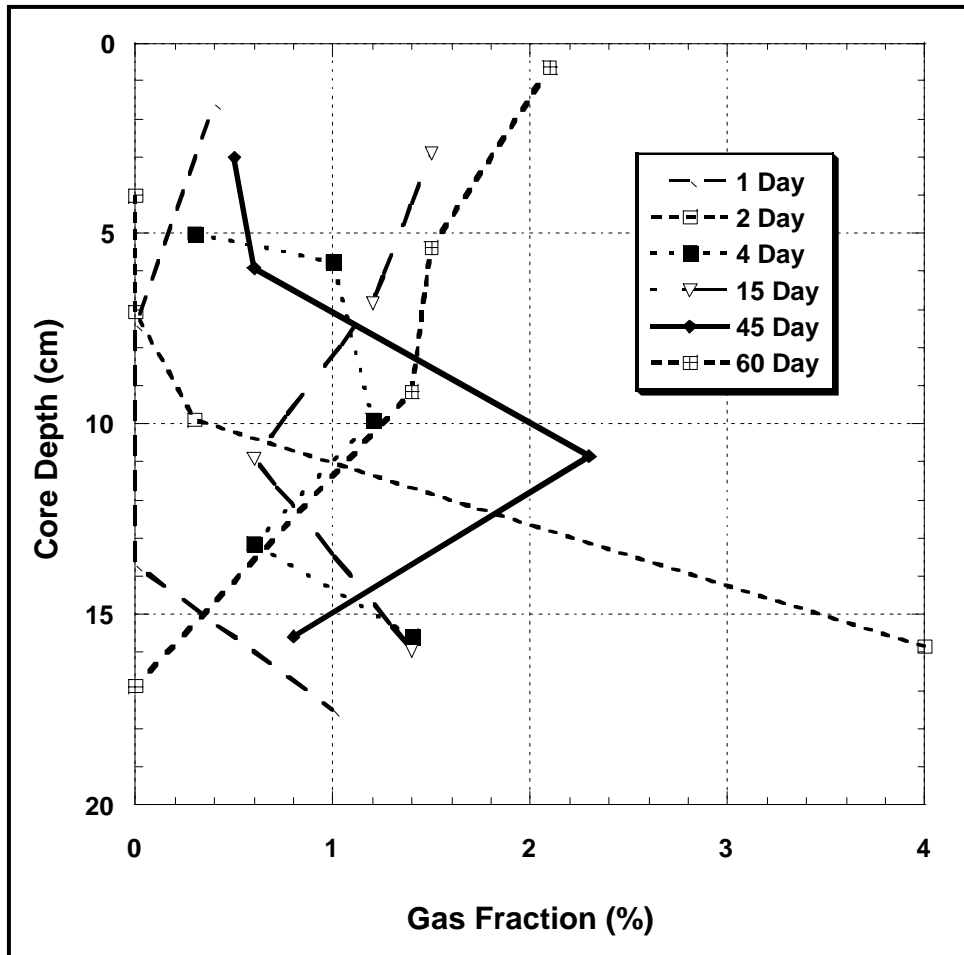


Figure 60. Gas fraction as a function of depth at times after deposition of 1, 2, 4, 15, 45, and 60 days

research indicates, as this Mobile sediment study implies, that most smectites are erosion resistant, then important conclusions can be extracted concerning dredged material behavior. Thus, for example, such a dredged material would be good for capping of contaminated material or for placement at an offshore disposal site where minimal dispersion is desired. In addition, a predominately sandy material with some smectite interspersed would be a poor choice for nearshore placement where beach nourishment is the goal. Further research will define sediment erosion rates based on mineralogy and other bulk properties. This will assist districts in predicting erosion rates for dredged material.

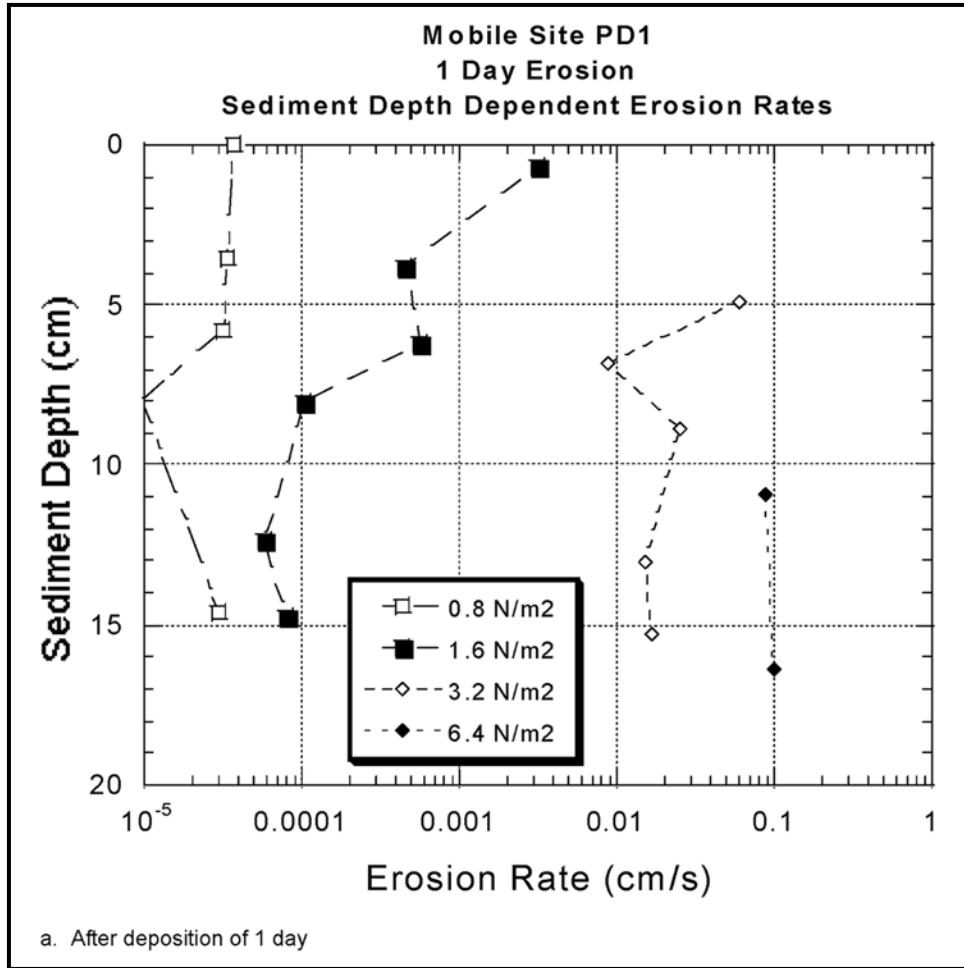


Figure 61. Erosion rates as a function of depth with shear stress (N/m^2) as a parameter at times (Sheet 1 of 4)

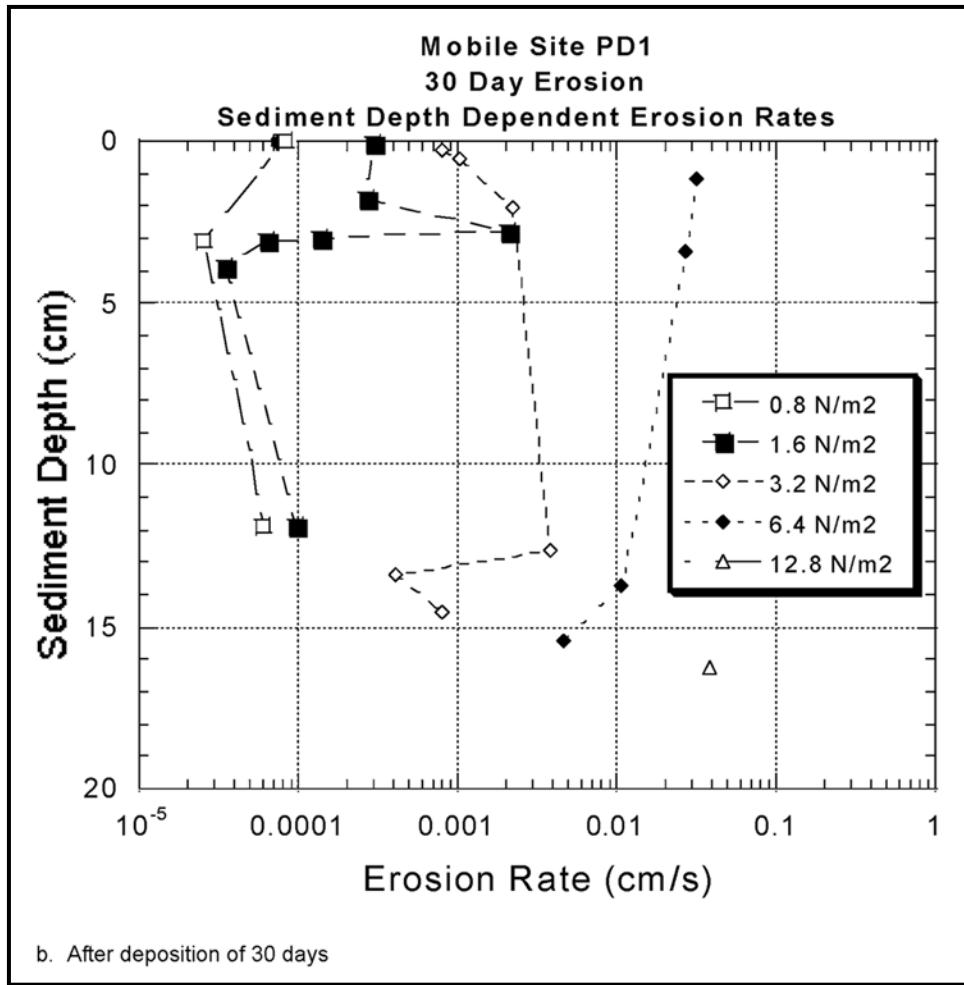


Figure 61. (Sheet 2 of 4)

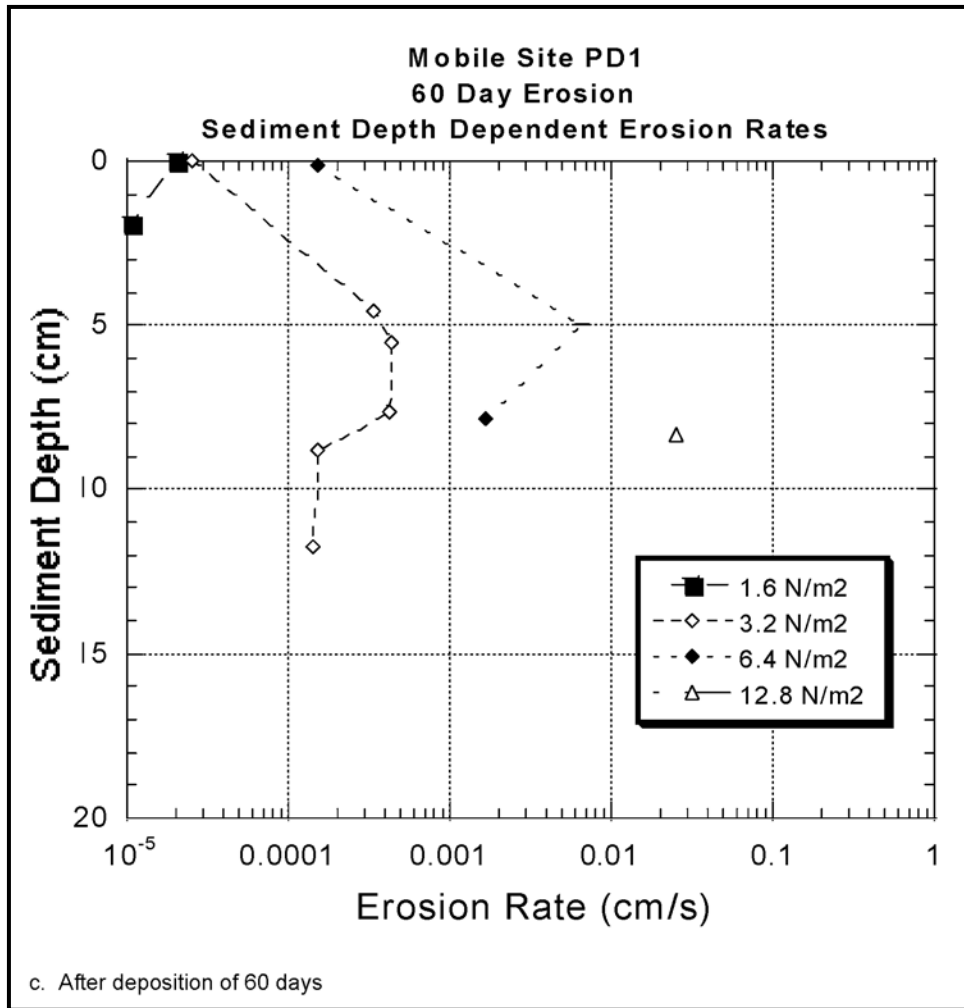


Figure 61. (Sheet 3 of 4)

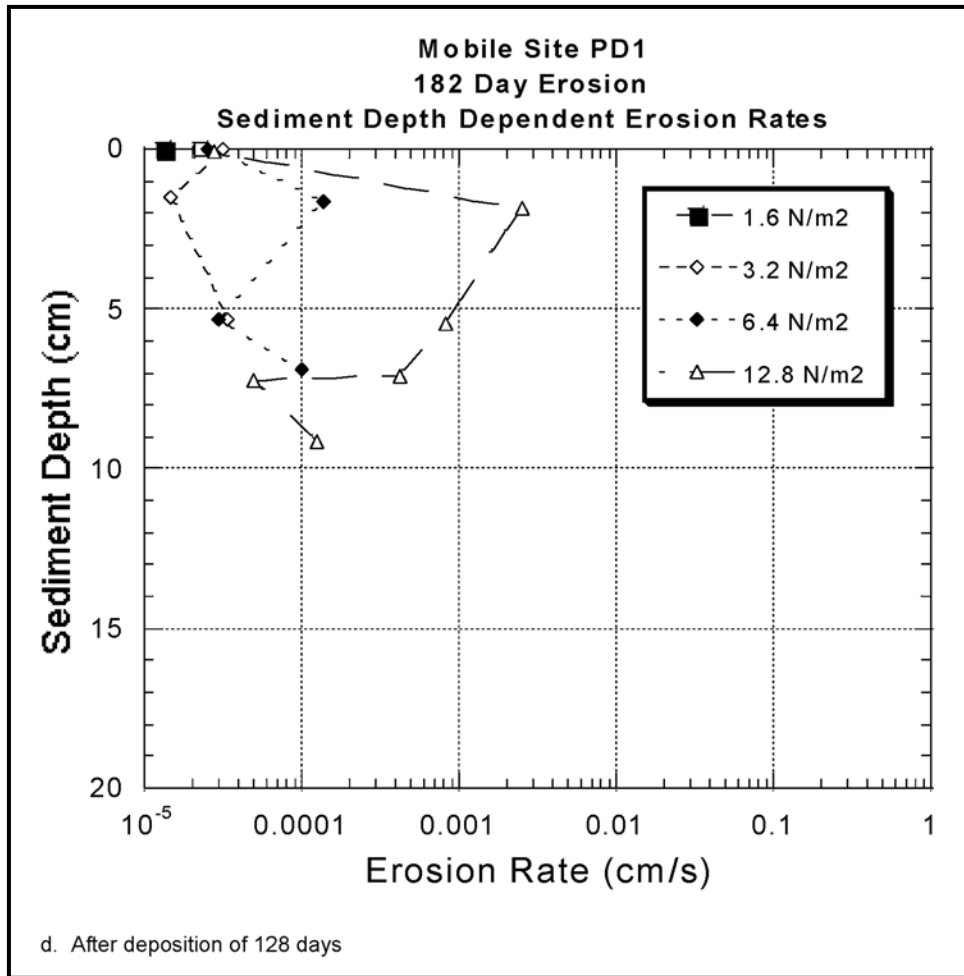


Figure 61. (Sheet 4 of 4)

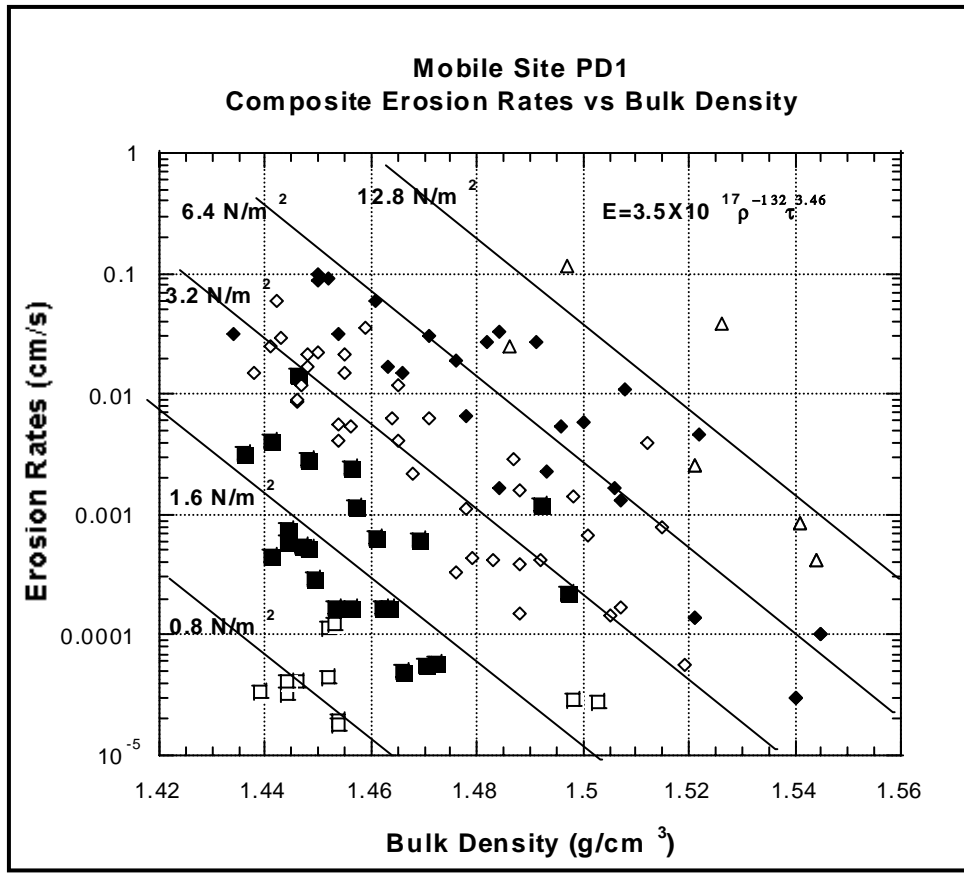


Figure 62. Erosion rates as a function of density with shear stress (N/m²) as a parameter. Straight lines are approximations by means of Equation 1

6 Conclusions

Wave, current, sediment samples, and multibeam bathymetry, have been collected to assess the long-term movement and changes in the mixed-sediment disposal mound. Analysis of the data has related the flow patterns and bathymetric change to the alteration in grain-size patterns from the native sediment to the placed material. Detailed multibeam bathymetry surveys were used to identify change in the bottom from before placement to after placement.

Native sediments in the area can be characterized as predominantly fine-grained, well-sorted, tan sands. Four native sediment types were identified based on sediment grain-size distribution curves and sediment statistics. Figure 63 shows the distinction in the mean grain sizes and sorting characteristics of four sediment types found at the study site. A fine sand component on the shallow

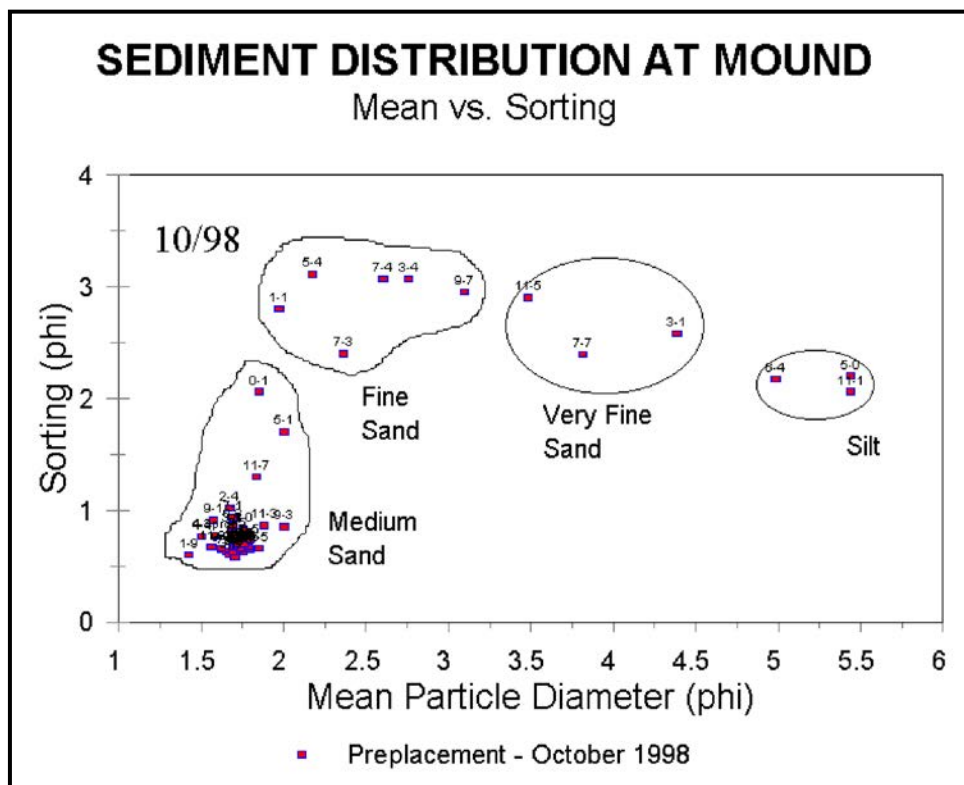


Figure 63. Mean versus sorting plot of native sediments showing four sediment types

edge of the ebb shoal is characterized by well-sorted sand-size material. More poorly sorted sands with an increase in finer, silty material was found on the side of the western ebb shoal. A native silt material was also present in the deeper depths around the base of the ebb shoal. Some of the native material was a bimodal mix with distinct peaks in the sand and silts size components and was poorly sorted due to the wide range in grain sizes in the samples.

The placement operation created several irregular peaks within the distinct mixed-sediment mound area, identified by the shift in the -9.1-m (-30-ft) contour gulfward. Surveys showed that some of the placement also created mixed-sediment peaks in the scour trough and the area immediately to the east of the trough. This mixed-sediment from the Mobile River placed at the site had a consistency of black, fine-grained, cohesive sediment. The grain-size distribution of the dredged material was distinct from the native fine sand and silt material in that it had means in the silt range and was poorly sorted with some organic debris, along with sand and clay size material (Figure 64). The cohesive nature of this river material resulted in little change in material distribution during the dredging, hauling operation, and deposition from the split-hull barges. Sediment collected from the barge operation at the dredge site in the Mobile River changed little from the material at the placement site, collected within days of placement.

Two postplacement multibeam surveys and sediment sampling activities were used to evaluate the change in the mound over time. Difference maps

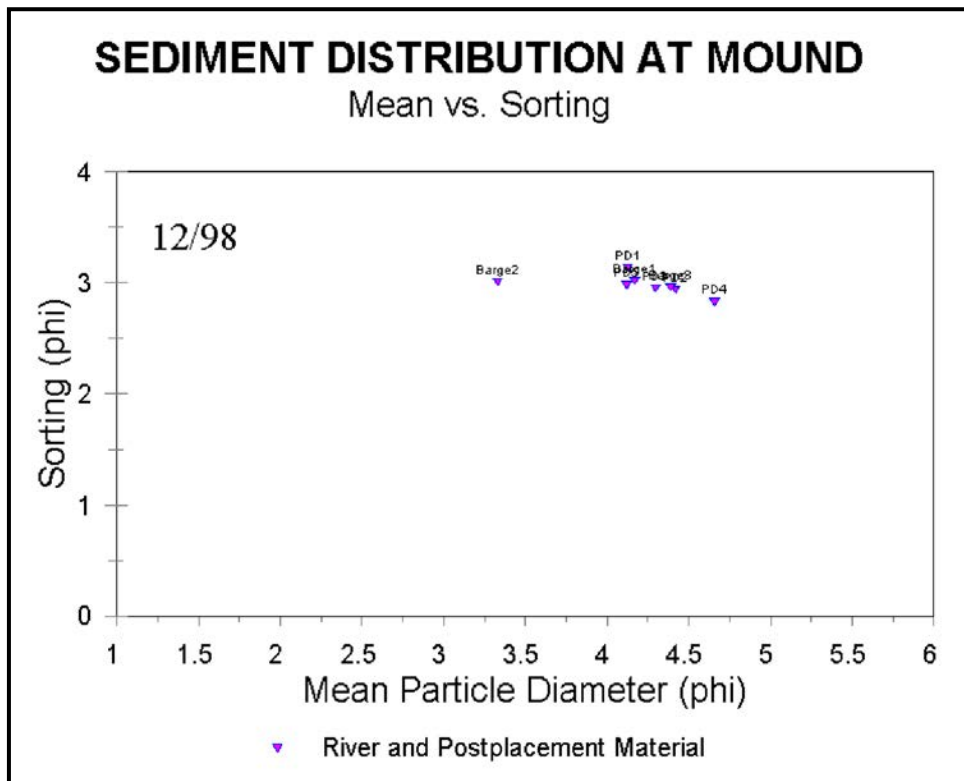


Figure 64. Mean versus sorting plot of Mobile River barge samples and immediate post placement sediments showing characteristic dredge material sediment type

One year after placement, there was little measured change in mound morphology. The largest change was to the north outside of the mix-sediment mound area where sand from dredging of the Mobile bar channel was placed on top of the ebb shoal. This material was composed mostly of fine sand material with some silt and no clay material. Changes in the sediment characteristics are shown in Figure 66 where the river samples were starting to mix with the native material. The well-sorted sand group was still distinct and for the most part unchanged. More samples were now in the silty sand group, which continued to encompass sand-size means that were more poorly sorted, due to the increase in finer material. Material easily identified as river sediments in the 6-month sampling now had more characteristics of the native sediment. Most of the finer mean grain-size samples had a coarser mean, but the sorting was still very poor, owing to the wide range in grain sizes from sand to clay size in the distributions. The bimodal group became less distinct and was merging with the native silt and river silt samples.

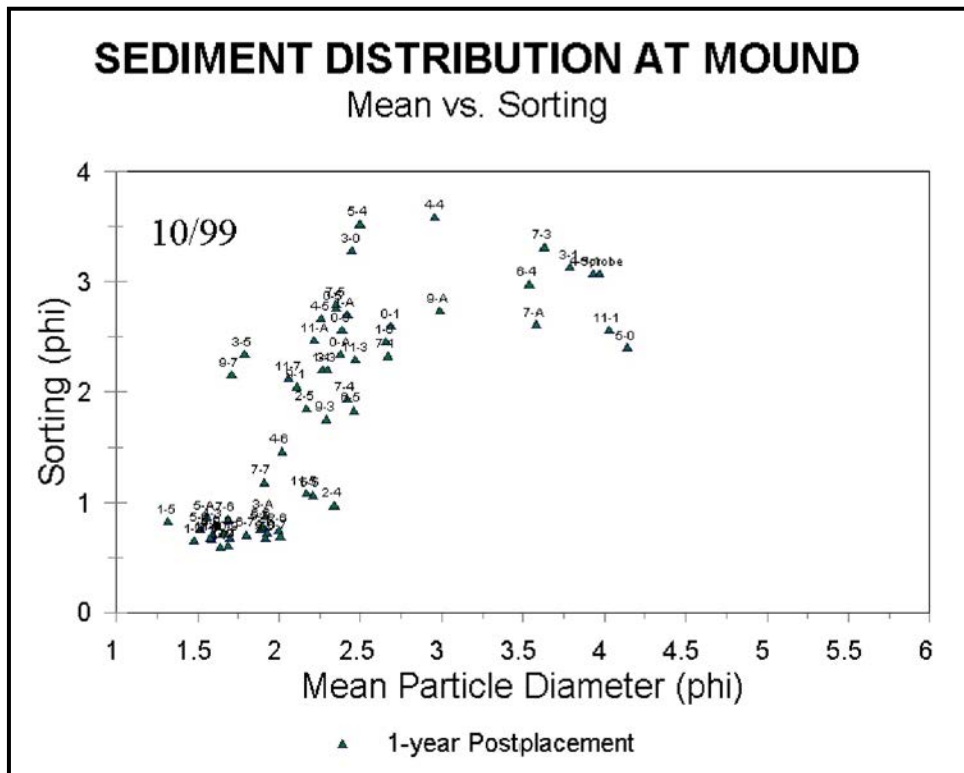


Figure 66. Mean versus sorting plot of mound area sediments showing change in 1-year postplacement sediment types

The spatial distribution of change in sediment grain-size distributions was constructed by comparing the entire distribution of each sample over time. Most of the samples had been collected twice, before and after placement, with many samples having three samples collected over the 1-year study time frame. A few samples had been collected four times near the mound. Five categories of sediment distribution change had been identified based on the frequency weight percent curves. The spatial pattern provided insight into the sediment mixing process (Figure 67). Most of the well-sorted fine sands that were collected above

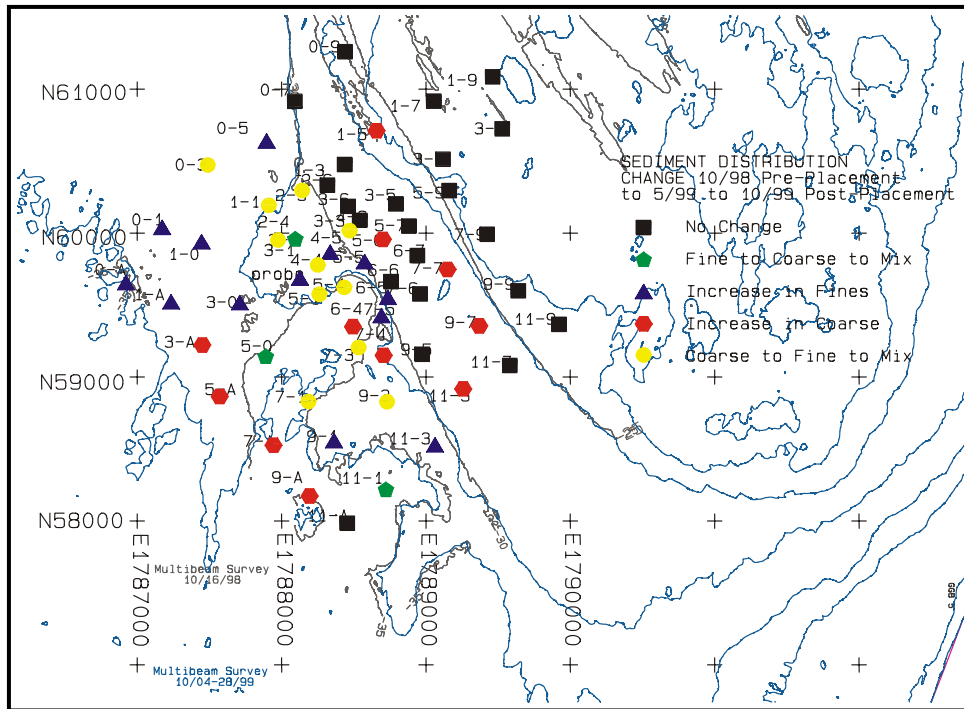


Figure 67. Map of change in sediment type from October 1998 to October 1999

the -9.1-m (-30-ft) depth contour had shown little change in their sediment distribution over the entire study period. These samples were above and to the north of the mixed-sediment mound. Figure 68 shows sample 5-1 (a representative sample in the no change group) that has a similar grain-size distribution in the preplacement (10/98), post-6-month placement (5/99), and post-1-year placement (10/99) samples. This uniform size distribution indicated that there was no influence of the mixed-river sediment in the area above the -9.1-m (-30-ft) depth contour on the ebb shoal and that the coastal processes had minimal effect on changing the depositional dynamics over this 1-year period. Sample 11-A at the extreme southeast corner of the sampling grid also showed no change in the sediment distribution. This sample was a silty sand material that was in deeper water below -10.7 m (-35 ft).

A second category of sediment change was an increase in coarser material after dredge material placement. Five such samples were located above the -9.1-m (-30-ft) depth contour and two were located on the nearshore shelf below the ebb shoal (samples 3-A and 5-A). These fine-sand samples increased the sand-size component and the distributions became coarser. Three native silt samples (6-4, 7-A and 9-A) in the scour trough vicinity increased the sand-size components of the distribution after dredge placement (as represented by sample 6-4 in Figure 69). Sample 7-4, a native bimodal silt and sand mix, received one of the errant river dumps. After 1 year, the fine sand portion of the sample increased forming a silty sand distribution. This sample was on the edge of the dredge material placement area and the location of the samples over time varied within a rough 36.6-m (120-ft) circular area, which may account for the change

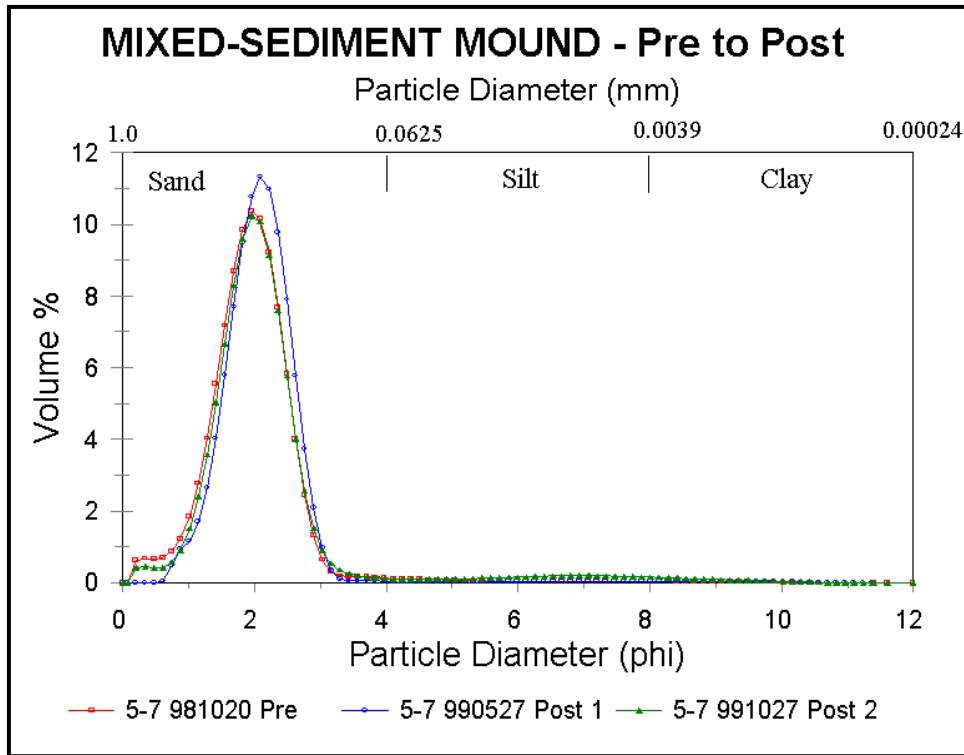


Figure 68. Example of grain-size frequency curves of the pre- and postdredge placement sediments in the *No Change* group

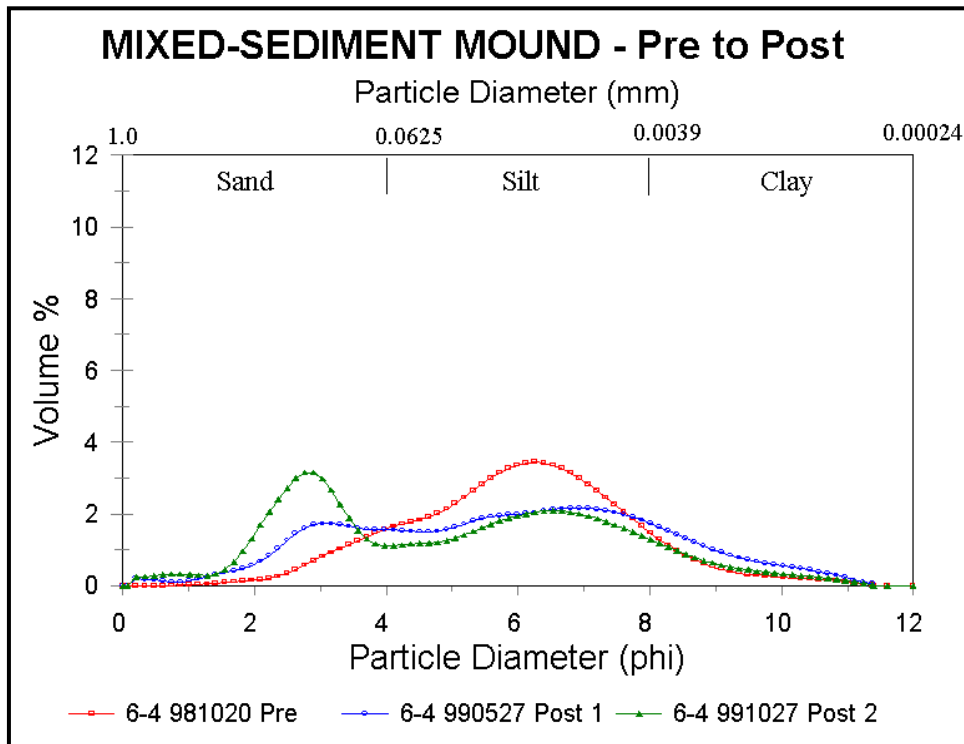


Figure 69. Example of grain-size frequency curves of the pre- and postdredge placement sediments in the *Increasing Coarse* group

as the different sampling periods may have sampled the dredge disposal at one time and the adjacent sand area the next.

Eleven samples in the placement area had a native sand-size distribution. The river sediment placed over the native sediment was the distinctive black silt. After 1 year, this class of sediment changed back to a mixed sand and silt mix, with a loss of the silt-size material and a gain in the sand-size material (as shown in a representative sample 4-4 in Figure 70). These samples retained much of the distribution of the river sediment but gained a larger sand component indicating that a mixing of the dredge material with the native sands had taken place. An exception to this mixing was found in Sample 9-3 to the south of the dredge material placement. This sample became slightly finer after the placement but retained a large amount of sand-size material. One year later the sand-size material had increased as the sample mixed.

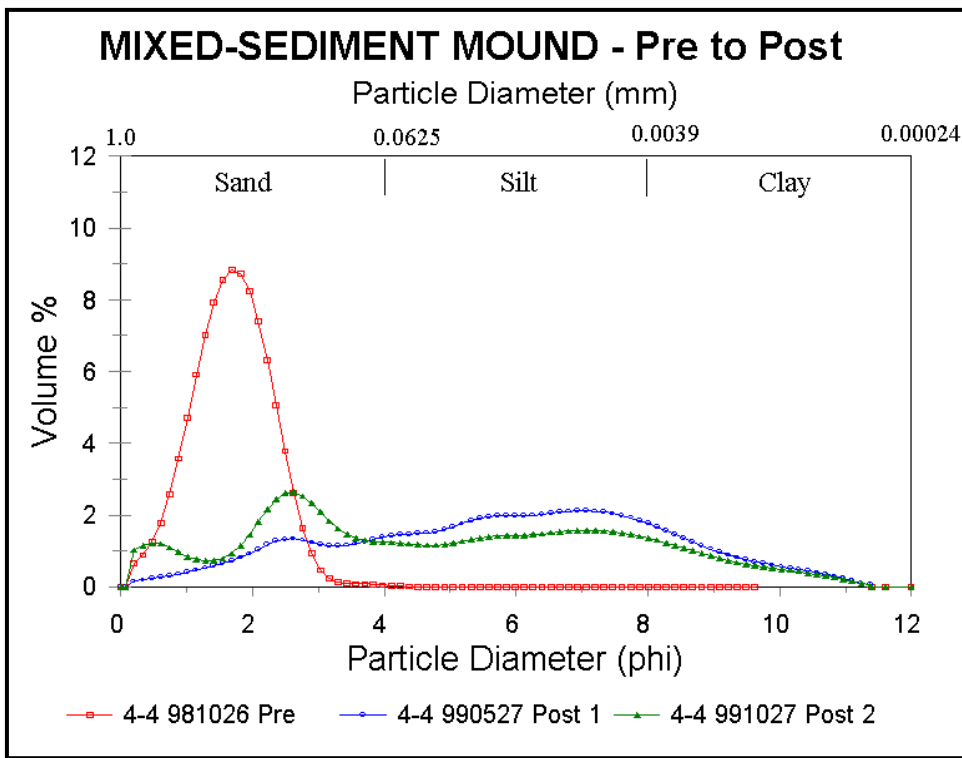


Figure 70. Example of grain-size frequency curves of the pre- and postdredge placement sediments in the *Coarse to Fine to Mixed* group

Five samples in the placement area and five samples to the west and south of the placement area gained finer material, and were classified as samples that increased their fine fraction of the distribution over the study period. Sample 3-0 illustrates this distributional change, changing from the native sand to a more dredge material like distribution 1 year later (Figure 71). The five samples in the placement area became even finer grained as time progressed. The samples to the west (outside the placement area) all appeared to pick up a fine silt portion after placement, possibly indicating a movement of the fine material to the west. Two samples to the east of the placement area (Samples 9-1 and 11-3) also became

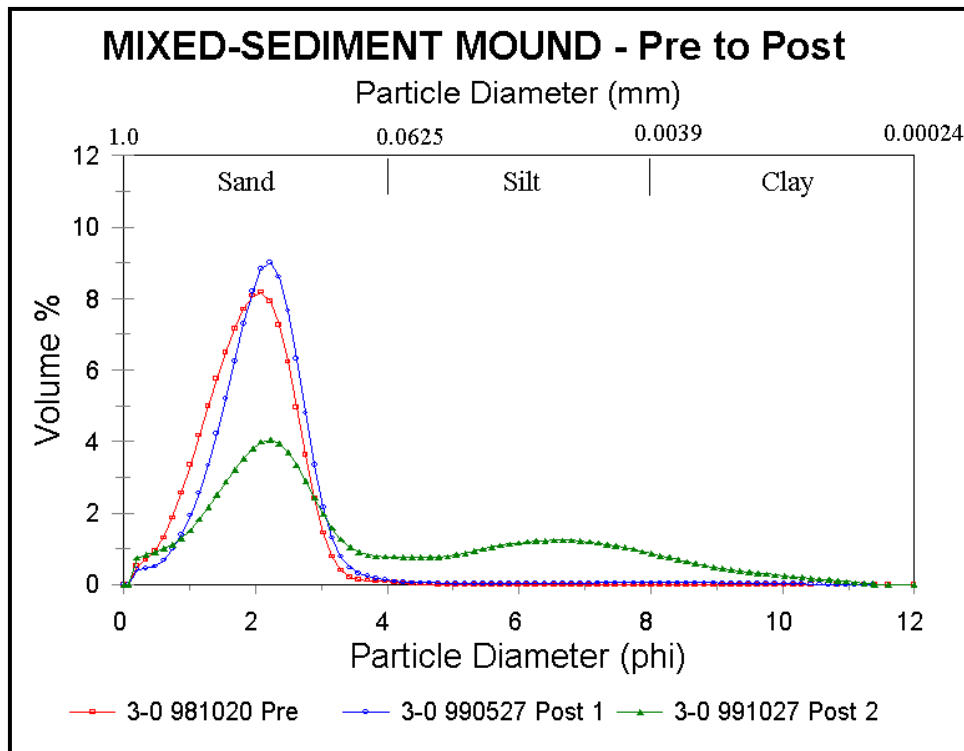


Figure 71. Example of grain-size frequency curves of the pre- and postdredge placement sediments in the *Increasing Fines* group

finer with a slight increase in silt-size material. Samples closest to the placement area received the most silt material as the distribution became finer. This may indicate that the finer material was moved to the west off the placement area and to the south associated with the filling in of the scour trough.

Three somewhat anomalous samples (3-1, 5-0 and 11-1) became coarser after the placement of the river material. These samples were all samples with a characteristic native silt distribution before dredge material placement. Sample 3-1 after the dump was a more well sorted, silty sand. One year after placement, the sample had characteristics of a mixed river sample with a small increase in fine sand (Figure 72). A possible explanation is that the May 1999 postplacement sample collected some native sand at the base of one of the dump mounds, reflecting more of a native fine sand sample. Sample 5-0 was on the west edge of the scour trough and had a native silt distribution. The May postplacement sample was collected higher up the side of the trough, which was more sandy. The October 1999 sample was a mix of the sand on the side of the trough wall, the native silt, and the dump material coming down to fill in the trough. Sample 11-1 was also a native silt material that increased in sand-size material after dredge placement. This sample was located in -11.6 m (-38 ft) of water at the base of the ebb shoal and near the scour trough base and away from any dredge material placement so the increase in sand-size material was possibly independent of any dredge placement and related to shelf/ebb delta edge sediment processes. One year after dredge material placement the sample had a mix of sand and silt material.

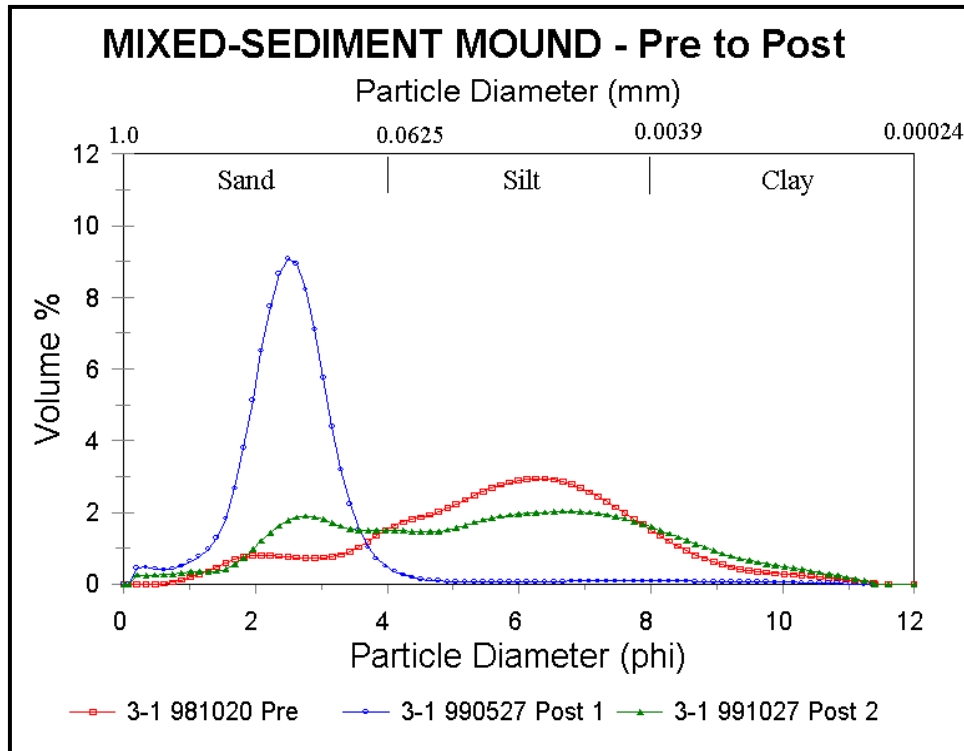


Figure 72. Example of grain-size frequency curves of the pre- and postdredge placement sediments in the *Fine to Coarse to Mixed* group

The pattern of minimal change measured in the bathymetry indicated that there was little change in the overall Mobile Bay entrance west ebb delta edge. Longer-term changes in the planform evolution of the placed material indicated that the individual mounds have been preserved over time. Some infilling of the scour trough created by Hurricane Georges has occurred as assessed with the detailed multibeam bathymetric surveys. The change in sediment distributions indicates there is little change in the bottom sediment composition of the sandy material above the -9.1-m (-30-ft) depth contour. In spite of the minimal change in bottom elevations, the sediment distributions indicate some change in the cohesive river sediment distribution over time. The samples to the west and south show the most change indicating the movement of the fines in those directions. The single ADCP current survey of the ebb and beginning of flood tidal cycle indicates the flow at the bed is low and only finer material would be placed in transport under normal tidal flow conditions. The direction of flow to the south and west is consistent with the sediment distribution change with fines moving to the west and south and down the scour trench axis. Normal current flow is too weak to actively move large portions of the native sand material or the cohesive river-origin dredge placement material. The formation of the scour trough during the hurricane, as well as shoaling in the Mobile bar channel, indicates that storm-induced currents are sufficient to transport all sediment found in the area. Storm processes appear to be the main player in modifying the coastal morphology and sediment distributions in this system. During the study period, there were no significant storms and the daily waves and currents have only slightly modified the mixed-sediment mound and surrounding area.

Bulk properties and erosion rates of the newly placed dredged sediments were measured and were found to be similar for all five sites at the Mobile Bay entrance mixed-sediment mound. These sediments had high concentrations of manganese and smectite. Both of these components caused significant increases in the critical shear stress and decreases in the erosion rates of the sediments compared to other sediments investigated. In particular, the high concentrations of Mn^{2+} precipitated as MnO_2 to form a surficial layer, which was very difficult to erode ($\tau_c = 1.5 \text{ N/m}^2$ (0.03 lb/ft²)). Even after this oxidized layer was eroded, the bentonite present acted to significantly reduce the erosion rates of the sediments that were below and were not oxidized.

Future numerical simulations of the study site using the LTFATE model will couple hydrodynamic data with observed bathymetric changes and additional sediment analyses to improve the accuracy of the model for predicting the fate of mixed-sediment dredged material placed nearshore. Data collected at this site provide useful input to the model. Given the cohesive nature of these dredged sediments and the low magnitude of the typical waves and currents at this site, a longer monitoring period will be required to capture changes in the mound. It appears that storm-induced changes are needed to affect significant sediment transport and change depositional patterns at the Mobile Bay entrance. However, the data collected and analyzed in this study provide a data point for model validation in that any sediment fate model should predict the condition of “no change.”

References

Bouws, E., Gunther, H., Rosenthal, W., and Vincent, C. L. (1985). "Similarity of the wind wave spectrum in finite depth water: 1. Spectral form," *J. Geophys. Res.*, 90(C1), 975-986.

Brigham Young University. (1995). "Surface-Water Modeling System," Version 5.0, Provo, UT.

Davis, J. E. (1992). "STWAVE theory and program documentation," Chapter 8, Coastal modeling system user's manual," Instructional Report CERC-91-1, Supplement 1, ed., M. A. Cialone, U.S. Army Engineer Waterways Experiment Station, Vicksburg, MS.

Federal Emergency Management Agency. (1999). "Building performance assessment report, Hurricane Georges," FEMA Report 338, March 1999, Washington DC.

Friedman, G. M. (1962). "On sorting, sorting coefficients and the lognormality of grain-size distributions of sandstones," *Journal of Geology*, 70, 737-753.

Gailani, J. Z., Kiehl, A., McNeil, J., Jin, L. and Lick, W. (2000). "Erosion rates and bulk properties of dredged sediments from Mobile, Alabama," DOER Technical Notes Collection (ERDC TN-DOER-N10), U.S. Army Engineer Research and Development Center, Vicksburg, MS.
www.wes.army.mil/el/dots/doer

Gotthard, D. (1998). "Three-dimensional, non-destructive measurements of sediment bulk density using gamma attenuation," Report, Department of Mechanical and Environmental Engineering, University of California, Santa Barbara, CA, 93106.

Hands, E. B. (1994). "Shoreward movement and other 5-year changes at the Sand Island Berms, Alabama," *Proceedings, 15th Western Dredging Association Conference*, San Diego, CA, 223-235.

Headquarters, U.S. Army Corps of Engineers. (2001). *Coastal Engineering Manual*, EM 1110-2-1100, Washington, DC.

- Hubertz, J. M. (1992). "A users guide to the WIS wave model, Version 2.0," WIS Report 27, U.S. Army Engineer Waterways Experiment Station, Vicksburg, MS.
- Hubertz, J. M., Brooks, R. M. (1989). "Gulf of Mexico hindcast wave information," WIS Report 18, U.S. Army Engineer Waterways Experiment Station, Vicksburg, MS.
- Jepsen, R., Roberts, J., and Lick, W. (1997). "Effects of bulk density on sediment erosion rates," *Water, Air, and Soil Pollution*, 99, 21-31.
- Jepsen, R., McNeil, J., and Lick, W. (2000). "Effects of gas generation on the density and erosion of sediments from the Grand River," *Jour. Great Lakes Research*, 26, 209-219.
- Jin, L., McNeil J., and Lick, W. (2000). "Effects of bentonite on sediment erosion rates," Report, Dept. of Mechanical and Environmental Engineering, University of California, Santa Barbara.
- Leenknecht, D. A., and Tanner, W. W. (1997). "Grid generation and data analysis for wave transformation models," *Proceedings, 4th Congress on Computing in Civil Engineering*, Philadelphia, PA.
- McNair, C. (1998). "The USACE Dredging Operations and Environmental Research (DOER) program," World Dredging Congress, Las Vegas, NV.
- McNeil, J., Taylor, C., and Lick, W. (1996). "Measurements of erosion of undisturbed bottom sediments with depth," *Jour. Hydr. Engrg.*, ASCE, 122(6), 316-324.
- Moritz, H. R. (1994). "User's guide for the multiple dump fate model, final report," Contract Report DACW39-94-M-1304, prepared for U.S. Army Engineer Waterways Experiment Station, Vicksburg, MS.
- Pratt, T. C., and Cook, D. S. (2001). "Draft HyPAS user's manual: A hydraulic processes analysis system," Technical Report CHL-01-1, U.S. Army Engineer Research and Development Center, Coastal and Hydraulics Laboratory, Vicksburg, MS.
- Pratt, T. C., and Stauble, D. K. (2001). "Shinnecock Inlet New York, site investigation, Report 3, selected field data report for 1997, 1998, 1999 velocity and sediment surveys," Technical Report CHL-98-32, U.S. Army Engineer Research and Development Center, Coastal and Hydraulics Laboratory, Vicksburg, MS.
- Resio, D. T. (1987). "Shallow-water waves. I: Theory," *J. Wtrway., Port, Coast., and Oc. Engrg.*, 113(3), 264-281.
- _____. (1988a). "Shallow-water waves. II: Data comparisons," *J. Wtrway., Port, Coast., and Oc. Engrg.*, 114(1), 50-65.

- Resio, D. T. (1988b). "A steady-state wave model for coastal applications," *Proc., 21st Coast. Engrg. Conf.*, ASCE, 929-940.
- Roberts, J., Jepsen, R., Gotthard, D., and Lick, W. (1998). "Effects of particle size and bulk density on erosion of quartz particles," *Jour. Hydr. Engr.*, 124(12), 1261-1267.
- Scheffner, N. W., Thevenot, M. M., Tallent, J. R., and Mason, J. M. (1995). "LTFATE: A model to investigate the long-term fate and stability of dredged material disposal sites: User's guide," Instruction Report DRP-95-1, U.S. Army Engineer Waterways Experiment Station, Vicksburg, MS.
- Smith, J. M., Resio, D. T., and Zundel, A. K. (1999). "STWAVE: Steady-state spectral wave model, Report 1, user's manual for STWAVE Version 2.0," Instruction Report CHL-99-1, U.S. Army Engineer Waterways Experiment Station, Vicksburg, MS.
- Stone, G. W., Wang, P., Pepper, D. A., Grymes, J. M., Roberts, H. H., Zhang, X., Hsu, S. A. and Huh, O. K. (1999). "Studying the importance of hurricanes to the Northern Gulf of Mexico coast," *EOS, Transactions, American Geophysical Union*, 80 (27), July 6, 1999, 301-305.
- Taylor, C., and Lick, W. (1996). "Erosion properties of Great Lakes sediments," Report, Department of Mechanical and Environmental Engineering, University of California, Santa Barbara, CA 93106.
- Thompson, E. F., Hadley, L. L., Brandon, W. A., McGehee, D. D., and Hubertz, J. M. (1996). "Wave response of Kahului Harbor, Maui, Hawaii," Technical Report CERC-96-11, U.S. Army Engineer Waterways Experiment Station, Vicksburg, MS.
- Tracy, B. A., and Cialone, A. (1996). "Wave information study, annual summary report, Gulf of Mexico 1994," WIS Report 35, U.S. Army Engineer Waterways Experiment Station, Vicksburg, MS.